Electron Temperature and Density Diagnostics in a Helium Glow Discharge

E. A. Den Hartog, T. R. O'Brian, and J. E. Lawler
Physics Department, University of Wisconsin, Madison, Wisconsin 53706
(Received 1 December 1988)

Two laser-based diagnostics are used to determine the density (n_e) and temperature (T_e) of low-energy electrons confined in the negative glow of a dc helium glow discharge. Each diagnostic yields an independent relation between n_e and T_e. From the intersection of these relations we find that $n_e = 5\times10^{11}$ cm^{-3} and $k_B T_e = 0.12$ eV for an abnormal cathode fall of 261 V in 3.50-Torr helium.

PACS numbers: 52.80.Hc, 52.20.Fs, 52.70.Kz

The negative-glow region of a dc glow discharge is characterized by a weak electric field and a high density of charged particles. This plasma is sustained by a low density of high-energy "beam" electrons which stream through the negative glow from the cathode fall region, causing excitation and ionization. The bulk of the electrons in the negative glow are low energy (<1.0 eV) and are held in the negative glow by a weak potential-energy well.[1] It is a common method to treat the electron energy distribution function as the sum of a Maxwellian describing the high density of low-energy electrons and a weak high-energy tail.[2]

In this Letter we describe a pair of laser-based diagnostics which together yield n_e and T_e for the low-energy electrons in the negative glow. Each diagnostic provides an independent relation between n_e and T_e. The first diagnostic, based on the endothermic electron collisional transfer between low Rydberg levels, yields a relation in which n_e decreases with increasing T_e. The second diagnostic, which has been reported previously,[1] is based on the spin conversion of helium metastables,

$$\mathrm{He}\,(2\,^1S)+e^-\rightarrow \mathrm{He}\,(2\,^3S)+e^-+0.79\ \mathrm{eV}. \qquad (1)$$

This diagnostic is based on an exothermic process and yields a relation in which n_e increases with increasing T_e. The intersection of these two relations yields the density and temperature of the low-energy electrons in the negative glow.

In the Rydberg-atom experiment a low Rydberg level is selectively populated with a laser. The electron collisional transfer rate from the level populated with the laser to a higher-lying Rydberg level is determined by measuring the ratio of the laser-induced fluorescence (LIF) signals from the two levels. Although high Rydberg levels do not survive sufficiently long to fluoresce in a typical discharge, low Rydberg levels do fluoresce. This rate can be written as the product of n_e and a rate coefficient which depends on T_e, thus determining a relationship between n_e and T_e.

A detailed description of the apparatus appears elsewhere.[1] The discharge used in this study is produced between flat circular aluminum electrodes 3.2 cm in diameter and separated by 0.62 cm. The electrodes are water cooled to minimize gas heating. For discharge operation ultrahigh-purity (0.999999) helium is slowly flowed through the system. A capacitive manometer monitors the pressure which is maintained at 3.50 Torr. The measurements reported in this Letter were made with a discharge current density of 0.846 mA/cm^2 corresponding to an abnormal cathode fall of 261 V.

The laser used is a pulsed, N_2-laser-pumped, narrow-band (0.2 cm^{-1}) dye laser, which is tunable over a wavelength range 360–700 nm. Frequency-doubling crystals are used to extend this range so that Rydberg levels may be excited out of the $2\,^3S$ metastable level. A cylindrical lens is used to focus the frequency-doubled light between the electrodes giving a spatial resolution of $\sim$0.2 mm. Spatial maps are made by translating the discharge on a precision translation stage.

Laser-induced fluorescence is collected in a direction mutually perpendicular to both the laser axis and the discharge axis. A lens is used to focus the fluorescence onto the 0.25-mm slits of a compact (0.2 m) monochromator which is used to isolate the desired fluorescence. The light is detected with a photomultiplier tube. The photomultiplier signal is amplified 100× and recorded with a Transiac 2001S digitizer with a 4100 averaging memory interfaced with an IBM PC.

Rydberg levels with the same principal quantum number "n" but different "l" are highly coupled by neutral collisions at 3.5 Torr. Excitation of the np level is effectively excitation of the entire n manifold with the populations of the various orbital angular-momentum levels being proportional to their degeneracy. The collisional transfer rate between two Rydberg manifolds is determined by measuring the ratio of their LIF signals when the lower-lying manifold is populated with the laser. Three such collisional transfer rates are studied. When the laser is tuned to the $2\,^3S$-$5\,^3P$ transition, fluorescence from $5\,^3D$-$2\,^3P$ and $6\,^3D$-$2\,^3P$ transitions is mapped, yielding the $n=5$ to 6 collisional transfer rate. When the laser is tuned to the $2\,^3S$-$6\,^3P$ transition, fluorescence from the $6\,^3D$-$2\,^3P$, $7\,^3D$-$2\,^3P$, and $8\,^3D$-$2\,^3P$ transitions is mapped yielding both the $n=6$ to 7 and $n=6$ to 8 collisional transfer rates. Figure 1 shows a map of the ratio of LIF from $n=7$ to that from $n=6$,

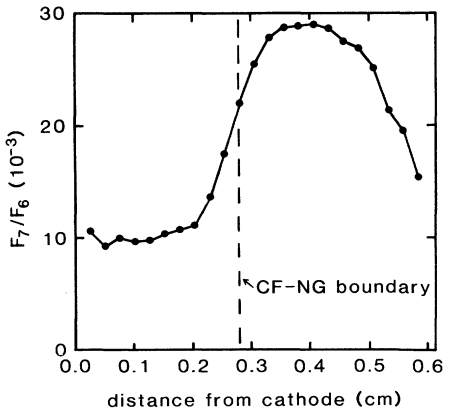

FIG. 1. Ratio of LIF signal from $n=7$ to that from $n=6$ vs distance from the cathode.

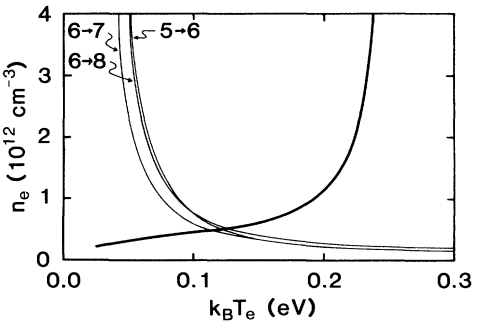

FIG. 2. Electron density vs electron temperature for the low-energy electrons in the negative glow. The three light lines arise from the Rydberg-atom diagnostic. The bold line arises from the metastable analysis.

when $n=6$ is populated with the laser. The position at which the cathode-fall field extrapolates to zero is indicated on the plot by a vertical dashed line. This is the cathode-fall–negative-glow (CF-NG) boundary. The enhancement of $n=7$ fluorescence to the right of this boundary is due to low-energy electron collisions in the negative glow.

The short duration (3 nsec) laser pulse produces an initial excess population $N_n(0)$ in the manifold having principal quantum number n. The decay is described by a single exponential because of the weak coupling between adjacent manifolds. The decay rate, τ_n^{-1}, includes both collisional and radiative processes. Under the same conditions the population $N_{n'}(t)$ of a higher-lying manifold n' is described by the rate equation

$$dN_{n'}(t)/dt = -N_{n'}(t)/\tau_{n'} + R_{nn'}N_n(t) ,$$

where $\tau_{n'}^{-1}$ is the depopulation rate of the n' manifold and $R_{nn'}$ is the rate for collisional transfer from manifold n to n', including both neutral and electron collisions. The solution to this equation is

$$N_{n'}(t) = \frac{R_{nn'}N_n(0)}{\tau_{n'}^{-1} - \tau_n^{-1}}(e^{-t/\tau_n} - e^{-t/\tau_{n'}}) .$$

The ratio of time-integrated fluorescence from the n' manifold to that from the n manifold is

$$\frac{F_{n'}}{F_n} = \frac{A_{n'd\text{-}2p}\int N_{n'}(t)dt/(n')^2}{A_{nd}\text{-}2p\int N_n(t)dt/n^2} ,$$

where A is a transition probability for a $d \rightarrow 2p$ transition and the observed fluorescence transitions are optically thin. After substituting and carrying out the integrals, $F_{n'}/F_n$ is given by

$$\frac{F_{n'}}{F_n} = \frac{n^2 A_{n'd\text{-}2p}R_{nn'}\tau_{n'}}{n'^2 A_{nd}\text{-}2p} .$$

This relation expresses the collisional transfer rate in terms of the measured ratio of fluorescence.

The manifold lifetime $\tau_{n'}$ is measured *in situ*. This is done by driving the $2\,^3S$-$n'\,^3P$ transition with the laser and collecting $n'\,^3D$-$2\,^3P$ fluorescence as described for the fluorescence mapping. The fluorescence decay is time resolved using a PAR 162/163 scanning boxcar integrator and plotted. Table I shows the results of measurements of $\tau_{n'}$ and the measured $R_{nn'}$ for the three different $n \rightarrow n'$ excitation transfers being studied. Because of the spatial asymmetry, the values of $R_{nn'}$ are quoted separately for the cathode fall and for the difference between the peak negative-glow signal and cathode fall. The electron density is negligible in the cathode fall and so $(R_{nn'})_{cf}$ is interpreted as the collisional transfer rate due to neutral collisions. The neutral transfer rate will be uniform throughout the discharge because the neutral density is uniform. The excitation transfer rate attributable to low-energy electrons in the negative glow is the difference between the rate in the negative glow and that in the cathode fall: $(R_{nn'})_{ng} - (R_{nn'})_{cf}$.

The measured electron collisional transfer rate can be expressed as the product of a temperature-dependent rate coefficient and the electron density n_e. We use the analytical formula given by Vriens and Smeets[3] for the rate coefficient. The resulting relations between electron density and temperature are shown as the thin lines in Fig. 2 for each of the collisional transfer rates measured.

TABLE I. Measured quantities $\tau_{n'}$ and $R_{nn'}$ for the three collisional transfer processes studied. The last column is the excitation transfer rate due to low-energy electron collisions in the negative glow.

$n \rightarrow n'$	$\tau_{n'}$ (10^{-9} sec)	$(R_{nn'})_{cf}$ (10^5 sec^{-1})	$(R_{nn'})_{ng} - (R_{nn'})_{cf}$ (10^5 sec^{-1})
$5 \rightarrow 6$	29.1	2.0	3.5
$6 \rightarrow 7$	30.8	6.0	11.1
$6 \rightarrow 8$	33.9	1.2	4.6

The metastable-atom diagnostic is carried out under the same discharge conditions as the Rydberg-atom diagnostic. The $2\,^1S$ and $2\,^3S$ metastable densities are measured as functions of axial position in the discharge. The diagnostic is based on the observed suppression of $2\,^1S$ metastables in the negative glow due to the metastable spin conversion reaction of Eq. (1). An analysis of metastable transport and kinetics in the discharge yields a net rate for the above reaction. From this rate a second relation between n_e and T_e is determined.

The metastable density measurements are made in two steps: (1) LIF is used to make maps of relative metastable densities, and (2) absorption measurements are made to put absolute scales on the density maps. The $2\,^1S$ metastables are mapped by driving the $2\,^1S$-$3\,^1P$ transition at 501.6 nm with the laser and observing $3\,^1D$-$2\,^1P$ fluorescence at 667.8 nm. The $2\,^3S$ metastables are mapped by driving the $2\,^3S$-$3\,^3P$ transition at 388.9 nm with the laser and observing $3\,^3S$-$2\,^3P$ fluorescence at 706.5 nm. These laser transitions do not require frequency doubling. The collimated laser is incident on a 0.25-mm slit which is imaged 1:1 into the discharge. Fluorescence collection and signal processing is much the same as for the Rydberg-atom experiment with the substitution of interference filters for the monochromator as a spectral filter.

The laser absorption measurements, needed for determining an absolute scale for the density maps, are made using the same laser transitions as the LIF measurements. The laser bandwidth is reduced to 500 MHz by introduction of an etalon. Absorption measurements are made at the peak of the spatial profile with 0.50-mm resolution. Saturation of the transition is avoided by reducing the laser power with neutral density filters. The transmitted laser intensity is monitored with a photodiode detector. The photodiode signal is processed with a boxcar averager and plotted on a strip-chart recorder as the laser frequency is scanned through the transition. Metastable densities are determined from the integral over frequency of the natural log of the transmittance. Ten absorption measurements are averaged to determine each density. The results of the metastable density measurements are shown as points in Fig. 3.

The metastable maps are analyzed to determine the net rate of metastable spin conversion. The transport and kinetics of $2\,^1S$ and $2\,^3S$ metastables in the discharge are modeled using a pair of balance equations which are coupled differential equations,

$$D_s\frac{\partial^2 M_s}{\partial z^2}-\beta M_s^2-\beta M_s M_t-\gamma M_s N-\kappa n_e M_s+P_s=0\,,$$

$$D_t\frac{\partial^2 M_t}{\partial z^2}-\beta M_t^2-\beta M_s M_t+\kappa n_e M_s+P_t=0\,,$$

where $M_{s,t}$ is the metastable density, N is the density of ground-state atoms, n_e is the density of low-energy electrons, D is the diffusion coefficient, P is the production rate per unit volume, γ is the rate constant for singlet metastable destruction due to collisions with ground-state atoms, β is the rate constant for the destruction of metastables due to metastable-metastable collisions, κ is the rate constant for net destruction of singlet metastables due to low-energy electron collisions, and s and t subscripts indicate singlet and triplet metastables, respectively.[1] The first three loss terms in each equation are loss terms arising from diffusion and collisions between metastables. There is an additional loss term in the singlet equation arising from collisions with ground-state atoms. The fifth loss term in the singlet equation is due to the metastable spin conversion reaction (1) and a corresponding gain term is included in the triplet equation. Values of DN, γ, and β are taken from Phelps.[4] The temperature dependence of D is taken from Buckingham and Dalgarno[5] and that of γ is taken from Allision, Browne, and Dalgarno.[6]

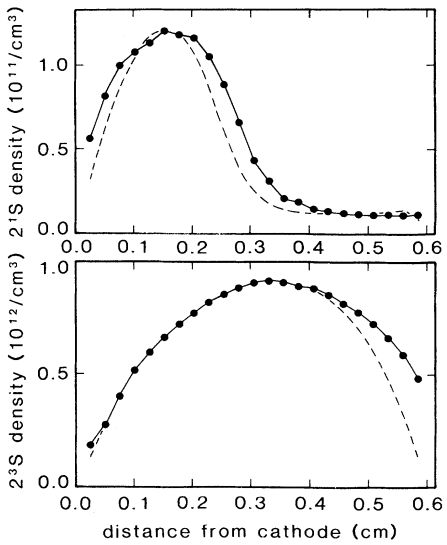

FIG. 3. $2\,^1S$ and $2\,^3S$ metastable densities vs distance from the cathode. The points are experimental measurements. The dashed curves are calculated densities using the fitting process described in the text.

The coupled equations are solved numerically for $M_s(z)$ and $M_t(z)$ and compared with the experimental results. In the calculation the spatial dependence of n_e is assumed to be a step function: zero in the cathode fall and uniform in the negative glow. The spatial dependence of the production terms is determined in Monte Carlo simulations to approximate a fundamental diffusion mode. Diffusion modes up to tenth order are included in the solutions to describe the spatial asymmetry of the $2\,^1S$ metastables. The values of P_s, P_t, and κn_e are varied until a good fit to the experimental metastable maps is obtained. The dashed curves of Fig. 3 are the calculated metastable densities determined in this manner. By this method, κn_e is found to be 7.0×10^4 sec^{-1}.

The rate constant κ_m for metastable spin conversion by room-temperature electrons was measured by Phelps.[4] The temperature dependence of the rate constant is $(T_e)^{-1/2}$ because the cross section scales as the inverse of the electron energy.[7] The κn_e determined from the metastable analysis must be considered an effective rate for metastable spin conversion since it accounts for both forward and reverse contributions of reaction (1). Setting κn_e equal to the expression for the forward rate minus the reverse rate we obtain

$$\kappa n_e = n_e[\kappa_m(0.025\ \text{eV}/k_B T_e)^{1/2} - (M_t/3M_s)\kappa_m(0.025\ \text{eV}/k_B T_e)^{1/2}\exp(-0.79\ \text{eV}/k_B T_e)] .$$

This expression yields a second relation between n_e and T_e which is shown as the bold line in Fig. 2. The intersection of the two relations yields $n_e = 5\times10^{11}$ cm^{-3} and $k_B T_e = 0.12$ eV for the electrons in the negative glow of a 261-V, 0.846-mA/cm^2 discharge in 3.50-Torr helium.

The uncertainty in the metastable-atom diagnostic is due mainly to neglect of the $2\,^1P$-$2\,^1S$ collisional-radiative coupling in the negative glow. Including this rather complex coupling could shift the curve from the metastable experiment to higher electron density, but this effect will be no greater than a factor of 2.[1,8] Assuming a factor of 2 uncertainty in the electron–Rydberg-atom rate coefficient also, then n_e will be between 4×10^{11} and 1×10^{12} cm^{-3}, and $k_B T_e$ will be between 0.07 and 0.16 eV. There are good prospects for improved knowledge of such rate coefficients.

Although the diagnostic based on the metastables may have limited applicability, it does have the distinct advantage that only electron collisions can couple the singlet and triplet He metastables. The Rydberg-atom diagnostic is broadly applicable since all atoms have Rydberg levels, and the level spacing may be chosen appropriately for the electron temperature of interest. Both laser-based diagnostics are noninvasive diagnostics and can provide good spatial and temporal resolution. They should be very useful in studying the structure of glow-discharge sheaths.

This research is supported by the Air Force Office of Scientific Research (AFOSR) and Grant No. AFOSR 84-0328.

[1]E. A. Den Hartog, D. A. Doughty, and J. E. Lawler, Phys. Rev. A **38**, 2471 (1988).

[2]Yu M. Kagan, C. Cohen, and P. Avivi, J. Appl. Phys. **63**, 60 (1988).

[3]L. Vriens and A. H. M. Smeets, Phys. Rev. A **22**, 940 (1980).

[4]A. V. Phelps, Phys. Rev. **99**, 1307 (1955).

[5]R. A. Buckingham and A. Dalgarno, Proc. Roy. Soc. London A **213**, 506 (1952).

[6]D. C. Allison, J. C. Browne, and A. Dalgarno, Proc. Phys. Soc. London **89**, 41 (1966).

[7]W. C. Fon, K. A. Berrington, P. G. Burke, and A. E. Kingston, J. Phys. B **14**, 2921 (1981).

[8]E. A. Den Hartog, Ph.D. thesis, University of Wisconsin–Madison, 1989 (unpublished).